VIII ECCOMAS Thematic Conference on Smart Structures and Materials
SMART 2017
A. Güemes, A. Benjeddou, J. Rodellar and J. Leng (Eds)

# STRUCTURAL DESIGN AND EXPERIMENTAL INVESTIGATIONS OF A SHAPE-ADAPTIVE SLAT FOR WIND ENERGY ROTOR BLADES

**OLIVER HUXDORF*, JOHANNES RIEMENSCHNEIDER†, PAUL LORSCH‡ AND MARTIN RADESTOCK§**

German Aerospace Center (DLR)
Institute of Composite Structures and Adaptive Systems
Lilienthalplatz 7, 38108 Braunschweig, Germany
e-mail: *oliver.huxdorf@dlr.de, †johannes.riemenschneider@dlr.de, ‡paul.lorsch@dlr.de, §martin.radestock@dlr.de

**Key words:** Wind Energy, Morphing, Adaptive Systems, Slat, Rotor Blade

**Abstract.** The trend towards larger rotor blades is still continuing, since the generated electrical power is proportional to the square of the blade length. However increasing rotor blade length will also increase the blades weight by the radius cube. Consequently mass induced loads such as centrifugal loads also increase. In addition larger blades lead to increased dynamic blade loads induced by vertical wind gradients and turbulent inflow conditions. A morphing slat that allows a dynamic gap variation between the slat's trailing edge and the main profile offers a great opportunity to reduce such fatigue loads. In order to show the proof of concept of such a shape-adaptive slat, a wind tunnel experiment was designed and executed. This paper presents the development of the shape-adaptive slat in wind tunnel scale. In order to ensure the fatigue behaviour a parameter study for the slat's design is done. The objective is to avoid a concentrated local strain maximum in the case of the deformed slat. As a next step, six slat segments are manufactured to investigate the deformation behaviour and to validate the simulations in a static experiment. The same segments are used to perform long-term fatigue investigations with dynamic slat deformations. Based on the experimental results a heat treated steel is selected to manufacture the final wind tunnel slat.

## 1 INTRODUCTION

The trend towards larger wind energy rotor blades is still continuing, since the generated electrical power is proportional to the square of the blade length. On the negative side larger wind energy rotor blades lead to increasingly and therefore critical dynamic blade loads at the blade root. These loads are induced by turbulent inflow conditions, vertical flow speed gradients due to the surface boundary layer and increased blade weights by radial length cubed in combination with changing blade orientations relative to the gravity. Consequently further blade up-scaling is limited by increased dynamic blade loads.

Recently investigations to the reduction of blade root loads by passive technologies such as bend twist coupling are done in [1, 2]. Another approach with more potential than passive methods and the possibility of direct lift control are active technologies. An overview of such technologies, their potentials and issues is given in [3]. Several investigations to camber variation with flexible trailing edges and conventional trailing edge flaps are done by the Danish Technical University (DTU) [4, 5, 6], Sandia National Laboratories (SNL) [7], Technical University Berlin [8] and Sandia National Laboratories together with FlexSys Inc. [9].

An alternative approach to camber variation is the use of shape-adaptive slats for wind energy rotor blades. This technology also offers the opportunity of direct lift control. The use of non-deformable rigid movable slats' is a well-known technology in aircraft applications. Existing patents for non-deformable wind energy rotor blade slats are proposed in [10, 11, 12]. Recent investigations with a fixed non-deformable auxiliary leading edge slat at a zero twist quasi-two-dimensional profile of type DU 97-W-300, which is described in [13], are done in [14]. Further investigations of [15] with a rigid retrofitted leading edge slat at the inner part of the 10 MW reference turbine RWT10, from the Danish LightRotor project, show the potential of leading edge slats' at wind energy turbines, especially the effect of an increased energy yield. The general effects of a non-deformable slat can be summarized with a delay in stall and an increased range of angles of attack in which the airfoil is working efficient. In contrast to a non-deformable slat a shape-adaptive slat also offers the opportunity of direct lift control.

In order to show the proof of concept this paper presents the development of a shape-adaptive slat with the possibility of a camber angle variation for wind tunnel investigations. Such a slat enables a changing gap size between the slat's trailing edge and the main profile. In case of a known incoming short-term inflow fluctuation as well as different flow speeds at various azimuth blade positions the slat's shape can be switched with the objective to control the aerodynamic forces and therefore to reduce dynamic blade root loads. This leads to an improved fatigue behaviour of the blade root and allows the design of larger and lighter blades. A short overview of the development procedure of this shape-adaptive slat is presented in [16]. A more detailed description of the development procedure is presented now in this paper.

## 2 GEOMETRY

As a first step to develop the shape-adaptive slat for wind tunnel investigations the non-deformed aerodynamic profile is defined in [17] in an optimization process. The starting point is the DU 91-W2-250 profile, which is shown in figure 1. Detailed information to this profile is given in [13]. The outcome of this study are two different aerodynamic profiles which are also shown in figure 1. The first one is characterized by a superimposed large cambering slat in front of the unmodified DU 91-W2-250 profile. The second profile is described by a modified main profile with a low cambering slat in front of them. The low cambering slat and the corresponding main profile are completely integrated in the original DU 91-W2-250 profile. Hence the second slat version is called "the integrated slat". Furthermore [17] compares the superimposed as well as the integrated profile in terms of lift and efficiency. Due to the better efficiency, the integrated slat is selected to develop the shape-adaptive slat for wind tunnel investigations.

The given geometry of the slat and the main profile is presented in figure 1. As shown the slat's suction side and the whole rear part of the main profile are identical with the original

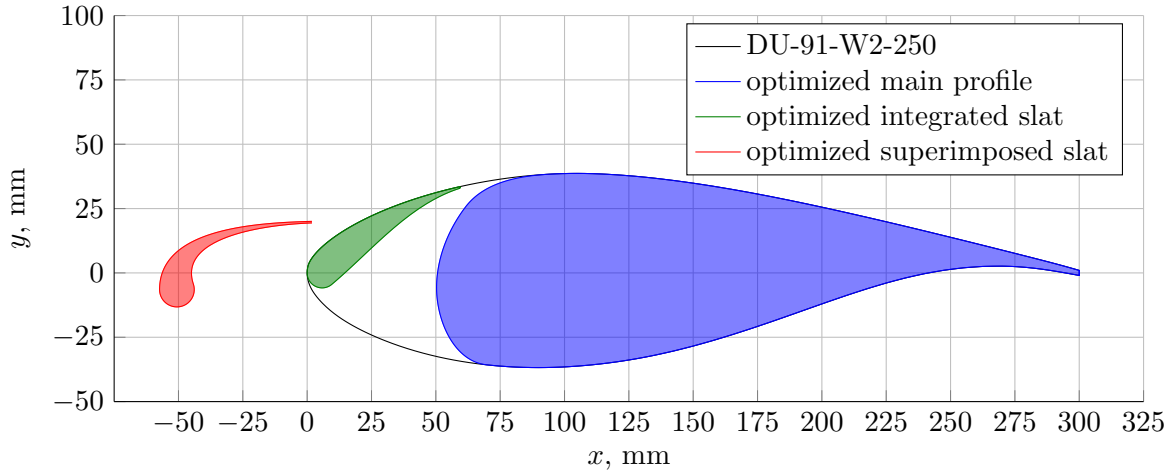


**Figure 1**: Integrated slat in red with the corresponding main profile in blue compared with the original DU 91-W2-250 profile in black. The geometry is presented in wind tunnel scale. The figure is based on data of [17].

DU 91-W2-250 profile. The main profile has a chord $c_{main}$ of 250 mm and a maximum thickness $t_{main}$ of 75 mm. The slat has a chord $c_{slat}$ of 69 mm and a maximum thickness $t_{slat}$ of 13.4 mm. In case of a non-deformed slat the shortest distance between the main profile and the trailing edge of the slat denoted as $g$ is 6.4 mm. The experimental aerodynamic investigations were executed in a wind tunnel from the University of Oldenburg. The measuring section of this wind tunnel has a width of 805 mm. Hence the main profile of the wind tunnel model has a span $s_{main}$ of 805 mm. In order to prevent friction between the side surfaces of the slat and the wind tunnel walls the slat has a span $s_{slat}$ of 803 mm.

## 3 REQUIREMENTS

As a next step the essential slat deformation requirements are defined. As a main requirement it has to be possible to close the gap completely. In order to be able to reduce dynamic blade loads the second essential requirement is a shape variation frequency $f$ of 5 Hz for the full amplitude. As a secondary requirement an additional gap enlargement beyond the non-deformed gap size should be possible.

## 4 CONCEPT DESCRIPTION

In order to design the shape-adaptive slat in wind tunnel scale, different structural concepts are investigated. Among others a concept with slat integrated pressurized cells as in [18] and [19], shape integrated piezoceramic actuators as used in [20] and the use of a kinematic chain as described in [21] are investigated and discussed. Each of these concepts has a significant disadvantage for the given requirements. The most promising and therefore the finally selected concept uses a kinematic mechanism as shown in figure 2. In order to ensure a continuous slat deformation as well as to minimize flow disturbances induced by the kinematics itself four span-wise positions are defined to deform the slat's compliant middle section as well as to fix

the slat's leading edge at the main profile (compare figure 2(a)). As shown in figure 2(b) the intermediate regions of these four positions allow an air flow between the pressure side of the slat and the main profile. The kinematics consists of a connecting rod (blue) and a shaft (brown). A stepping motor (not shown) is used to drive the shaft and therefore to deform the middle section of the slat. As a result the gap will be closed or opened.

In order to improve the fatigue behaviour, to reduce the necessary deformation forces and to reduce the resultant strain in case of a deformation the slat is designed as a hollow profile. Further fatigue improvements are realized with a slotted pressure side of the slat.

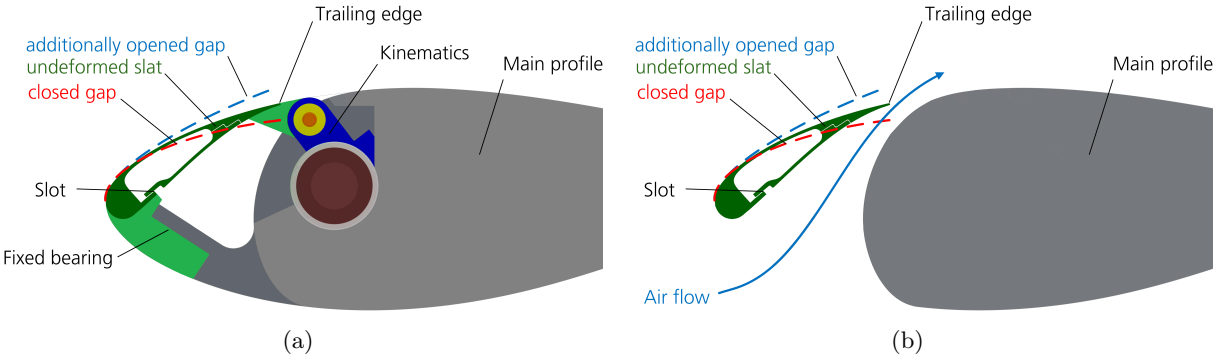


**Figure 2**: Working principle of the shape-adaptive slat with sketched deformed slat shapes. (a) Structural concept in the span-wise plane of the actuation stations. (b) Structural concept at the span-wise planes away from the actuation stations.

The presented concept of a shape-adaptive slat is developed for use on a scaled wind tunnel model. Future investigation deals with the up-scaling of the selected concept.

## 5 DESIGN PROCESS

This section presents the detailed design process of the slat. In a first step the slat's inner contour is optimized in a parameter study to minimize the resultant strains in case of a deformed slat and therefore to improve the fatigue behaviour. As a next step six identical slat segments are manufactured to investigate the deformation behaviour of the slat and to validate the generated FE models. Afterwards these segments are used for fatigue investigations. This section will be closed with a short description of the final wind tunnel model.

### 5.1 Parameter study for fatigue improvements

The objective of this study is to minimize the resultant maximum strain in case of a deformed slat and therefore to improve the fatigue behaviour as well as to ensure the fatigue strength during the whole wind tunnel measurements. This is achieved with a parameter study of the inner contour of the slats' suction side. The general objective is to spread a resultant possibly concentrated local strain maximum to the whole compliant middle section of the slat. In contrast to the soft requirement of an additional gap enlargement the possibility of a completely closed gap is a hard requirement. Consequently this load case is used for the following numerical investigations.

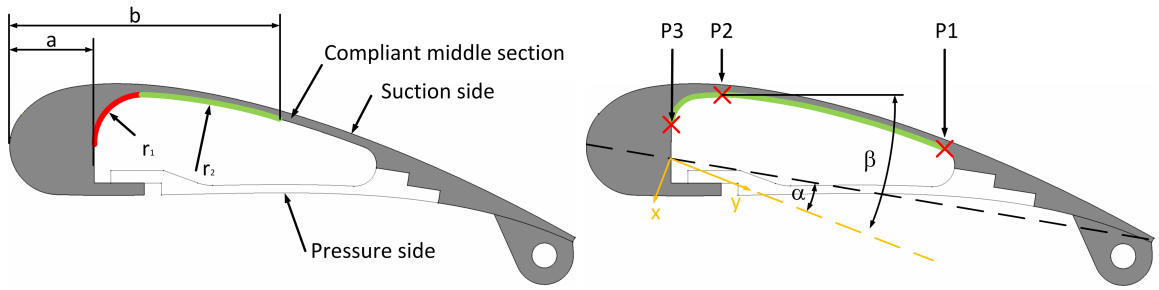


(a) (b)

**Figure 3**: Sketch of two different approaches to describe the inner contour of the slat's pressure side. (a) Two tangential radii as contour description. (b) Polynomial function as contour description.

In order to describe the slats inner contour two different approaches are used. The first approach uses two tangential radii to describe the inner contour and is shown in figure 3(a). In order to get a definite contour description the following boundary conditions are defined. Both radius $r_1$ and radius $r_2$ merge tangentially to each other and to the slats' front as well as rear part. The starting point of radius $r_1$ is defined with parameter $a$. The end point of radius $r_2$ is defined with parameter $b$. The contour variation is achieved with various values for the parameters $a$, $b$ and $r_2$. Parameter $r_1$ is defined as a result of the remaining three parameters and the associated boundary conditions.

As a second approach the inner contour is described with different polynomial functions of orders 5 to 12 and various corresponding coefficients $c_i$. A sketch of the approach is shown in figure 3(b). A definite polynomial contour is achieved with the following boundary conditions. First, the polynomial function is only considered between the $x$ coordinates of point $P1$ and point $P3$. The polynomial function is tangential to the slat's front part in point $P3$ as well as to the rear part in point $P1$. In order to achieve a contour variation the coordinates $x$ and $y$ of Point $P2$ and the slope $\beta$ in the same point are used as parameters. In order to generate full definite polynomials only six functional coefficients with $c_i \neq 0$ are used. For functions with orders higher or equal than 6 the four even leading coefficients as well as the linear and the absolute coefficients are used. In case of order 5 each coefficient is used to define the function. The polynomial functions of order 10 are identified as best contour description. This function type is used for the detailed parameter study.

In order to perform the parameter study a combination of different tools is used. The base is built with a parametric CAD - model in Catia. The parameter variations are realized with Matlab. For each parameter combination the CAD - model is updated by Matlab. The resultant slat's inner contour of each combination is exported to a parametric FE - model in Ansys. The numerical calculations are done with a two-dimensional FE - model of the slats' structure in plane of one actuation station (compare sketched plane

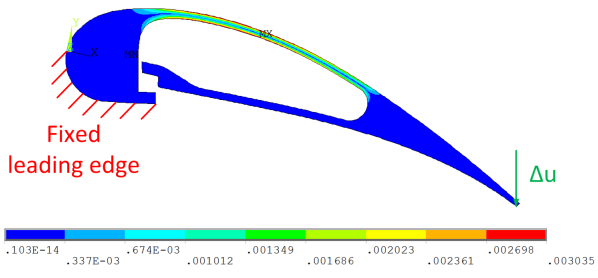


**Figure 4**: Resultant numerical strain distribution in case of a completely closed gap.

in figure 2(a)). The used FE - model is shown in figure 4. In order to simulate the expected loads the slats' leading edge is defined as fixed. The middle section deforms in consequence of the attached displacement $\Delta u$.

The best performing configuration in terms of minimized strains is achieved with a polynomial function of order 10. The resultant strain distribution is shown in figure 4. The maximum strain $\varepsilon$ is approximately 0.3 %. Based on this result and to ensure the fatigue strength of the wind tunnel model during the whole wind tunnel measurements a heat treated steel of type 30CrNiMo8 is used as the material for the wind tunnel model of the slat. This results in a mechanical stress $\sigma$ of 630 N/mm$^2$. Of course there is the potential for further strain reductions, for example with other contour descriptions, but due to the limited time this has to be explored outside of this project. Additional strain reductions could be reached with thinner slat skins, but the combination of the slats dimensions with milling as the manufacturing process leads to a minimum skin thickness $t_{skin}$ of 1 mm. Otherwise the risk of vibrations during the manufacturing process and therefore increased manufacturing inaccuracies is to high.

As shown in figure 4, the pressure side of the slat's skin is slotted. In case of a closed gap the pressure side's skin raises from the front part of the slat. This effect is also shown in figure 4. In case of an additional gap enlargement the pressure side's skin shores at the slat's front part.

### 5.2 Manufacturing

Based on the results above a pre version of the slat is designed. In a next step this design is used to manufacture six identical slat segments with a span $s$ of 40 mm. One slat segment is shown as an example in figure 5. As can be seen the force application point (connection with kinematics) is located in an extension of the slats' trailing edge. The slats' bearing is realized with two bolts putted in an extension at the slats' leading edge. The bolts are not shown.

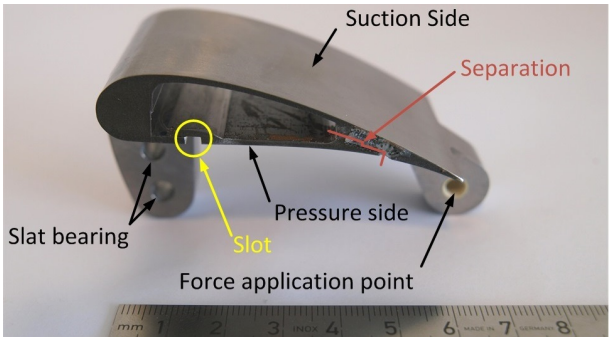


**Figure 5**: Manufactured slat segment.

In order to manufacture the slat segments the slats' suction and pressure sides are manufactured separately in a CNC milling process. Afterwards both sides are glued together. The same manufacturing process is used for the final wind tunnel model of the slat.

### 5.3 Static investigations

As next step one slat segment is used for static investigations. The objective is to determine the real slat's deformation behaviour, the resultant strain distribution, the necessary deformation forces to close the gap completely and to validate the generated numerical tools. The used experimental setup is shown in figure 6(a).

Two bolts are used to fix the slat's leading edge at a massive block. Another bolt is used to fix different gravity forces at the force application point. An optical measuring system called GOM ARAMIS$^{TM}$[22] is used to detect the deformation behaviour and the strain distribution

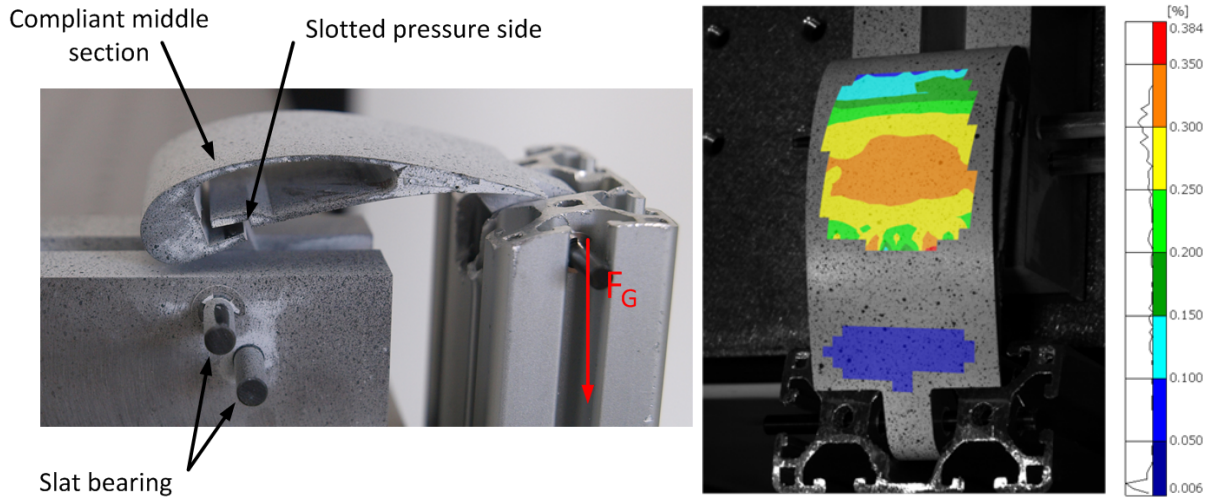


(a) (b)

**Figure 6**: Experimental setup to validate the resultant simulated strain distribution (left) with the resultant experimental strain distribution in the case of a fully closed gap (right).

for different load steps. As shown in figure 6(b) only the compliant middle section and the rear slat shortly before the trailing edge are measured, because of light reflections and system restrictions.

The determined shifting curve of the slat's trailing edge is sketched in figure 8. As can be seen the resultant shifting curve is not identical to the direction of the shortest gap between the slat's trailing edge and the surface of the main profile. In order to close the gap completely a displacement at the force application point $u_{close}$ of approximately 9 mm is required. The corresponding force $F_{close}$ is 120 N. The resultant maximum strain $\varepsilon_{close}$ is 0.34 %. It follows a deviation of 12 % compared to the numerical results of figure 4, which is in an acceptable range. The resultant mechanical stress $\sigma_{close}$ is 714 N/mm$^2$. The permitted maximum fatigue strength without a stress offset is figured out from the Smith diagram (diagram TB 3-1 in [23]) in figure 7 and is approximately 610 N/mm$^2$. Therefore the existing maximum mechanical stress is higher than the permitted fatigue strength without a stress offset. This means the fatigue strength for a dynamic shape variation with an amplitude of $u_{close} \approx 9$ mm is not allowed. The resultant maximum permitted stress for an additional gap

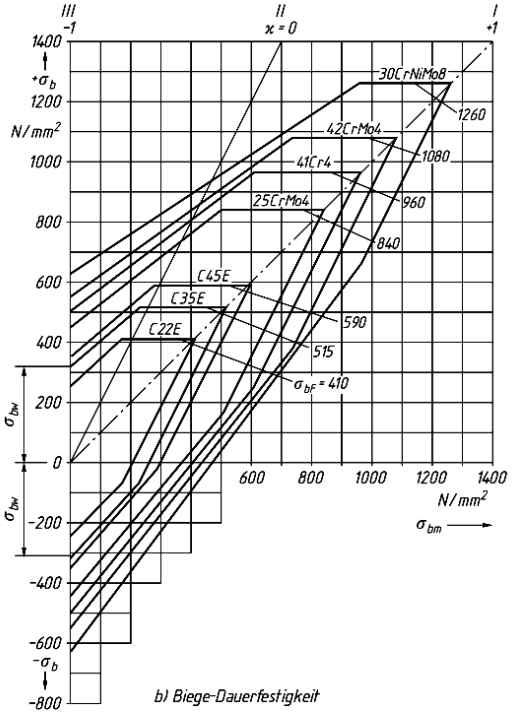


**Figure 7**: Smith diagram for different heat treated steels (diagram TB 3-1 in [23])

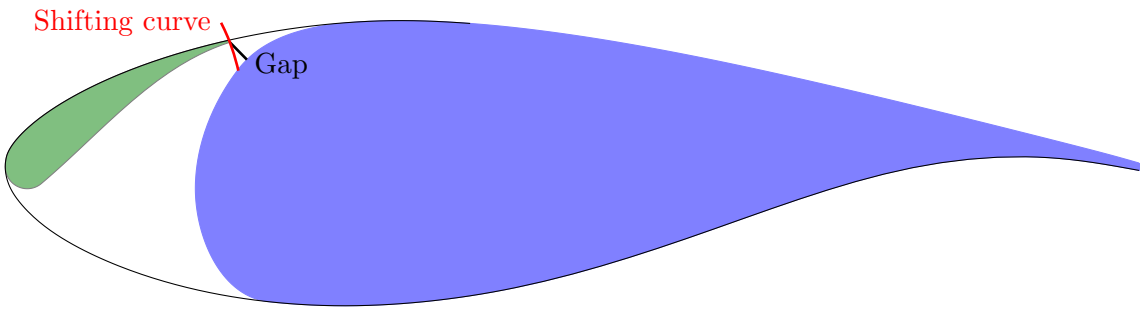


**Figure 8**: Resultant shifting curve of the slat's trailing edge due to different weight forces at the slats' force application point.

enlargement $\sigma_{open}$ is $-450\,\mathrm{N/mm^2}$ and is also acquired from figure 7. The corresponding permitted gap enlargement $u_{open}$ to the full closed gap is calculated approximately with a proportion equation of $u_{open} = (\sigma_{open}/\sigma_{close}) \cdot u_{close}$. Using this equation an additional gap enlargement $u_{open}$ of approximately 5.7 mm directly at the force application point results.

### 5.4 Fatigue investigations

As described above the next step are fatigue investigations to ensure the fatigue strength during the wind tunnel measurements. Therefore a classic fatigue test up to $1 \cdot 10^6$ cycles is performed for the slat segments. The opening and closing of the gap, as sketched in figure 2, is one load cycle. The closing force $F_{close}$ of 120 N is applied to simulate the complete closing of the gap. The used test rig simulates a continuous opening and closing of the gap. This is done by an eccentric shaft with a variable stroke that drives a connection rod, which is directly linked to the trailing edge of the slat. An electric motor drives the shaft at approximately 300 rpm, which leads to a loading frequency of 5 Hz. As the eccentric shaft induces a constant stroke within the fatigue test, the test is deflection controlled. The opening and closing force that must be reached have to be calibrated with a few cycles before the fatigue test starts. As the stroke is then locked, the resultant force is monitored during the fatigue test. Any change in the mechanical behaviour of the slat can then be seen in a change of the resultant force. Additionally several strain gauges were applied to the slats to monitor any changes in the strain distribution on the slats.

In total five slats were tested. Because of the limited amplitude of the used test rig each slat segment is investigated with different closing and opening forces to cover all expected fatigue loads. This paper presents the results of slat segment 4. This segment is tested with a maximum force $F_{max}$ of 123 N (blue curve) which is close to the closing force $F_{close}$ with 120 N and a minimum force $F_{min}$ of $-11$ N (red curve). Figure 9 shows the resultant forces over the entire fatigue test up to $1 \cdot 10^6$ cycles.

It can easily be seen that the resulting force barely changes over the course of the test. Within the first hundred load cycles the resultant force changes the most. This is a result of the mechanical settling of the test rig. After that settling any barely change of the resultant force are visible. This behaviour was proven by examining the measurements of the strain gauges,

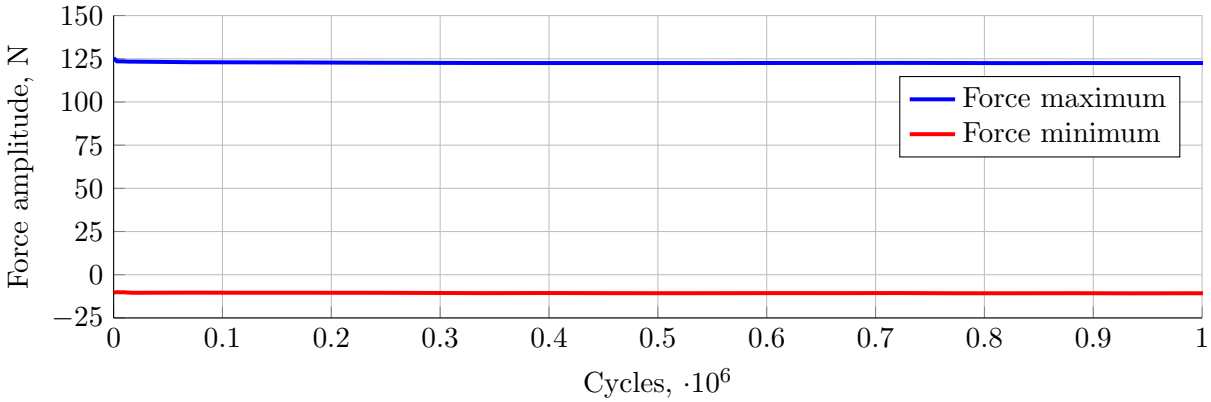


**Figure 9**: Envelope curve of the maximum and minimum forces that resulted from the fatigue loading of slat segment 4.

that were applied to the upper surface of the slat. Thereby and in combination with the results of the remaining four slat segments it can be stated, that no measurable damage occurred in the slat and the operational stability is given.

After the successful test, the strain gauges are removed from the slat to examine the surface in detail. A photograph of the slat is given in figure 10. The remnants on the surface are the soldering points from the strain gauges that could not be removed without damaging the slats' surface. No cracking or roughening is found on the slat. Severe mechanical damage due to fatigue could not be found. After the optical examination several bores are applied to the slat for installation tests of pressure taps. These bores can also be seen in figure 10.

In total, all slats showed this type of behaviour. No noticeable change in the resulting force was observed. In order to simulate an additional gap enlargement one slat segment is tested with a maximum force $F_{max}$ of 77 N and a minimum force $F_{min}$ of $-75$ N. The resultant stress ratio is $R = \sigma_{min} / \sigma_{max} \approx -1$, which is known to be a severe load case in fatigue. This proves, beyond the already shown operational stability, structural reserves against fatigue.

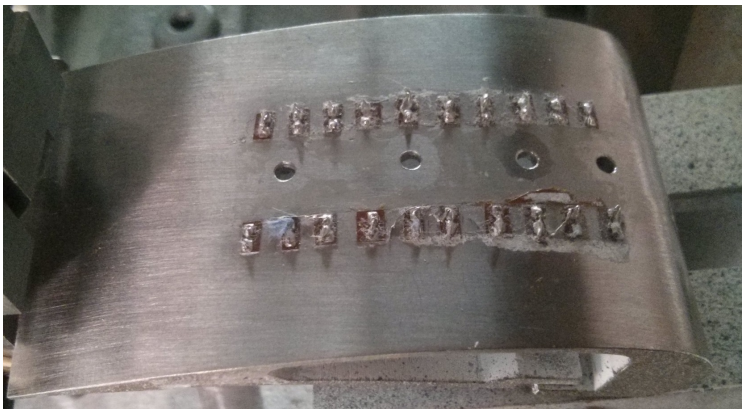

**Figure 10**: Slat segment 4 after the fatigue test with approximately $1 \cdot 10^6$ cycles. The bores visible in the picture were applied after the fatigue test.

## 6 WIND TUNNEL MODEL

Based on the results above the final wind tunnel model with the slat and the corresponding kinematics as well as additional parts are designed. Also the stepping motor to drive the shaft is selected. Afterwards the final wind tunnel model with a span $s_{main}$ of 805 mm and the corresponding slat with a span $s_{slat}$ of 803 mm are manufactured. The finally manufactured wind tunnel model with the shape-adaptive slat in front of the main profile is shown in figure 11.

Compared to the slat segments the slat's bearing is redesigned with the objective of reduced flow disturbances generated by the slat mounting itself. Hence two screws in chord direction instead of two bolts in span wise direction are used. An additional bolt in chord direction is used for deformation induced shear loads and to ensure identical slat position after possible reassemblies. The thickness at each slat mounting is 15 mm. The distance between the middle planes of the actuation stations is 200.75 mm.

**Figure 11**: Manufactured wind tunnel model with the non-deformed shape-adaptive slat in front of the main profile.

## 7 CONCLUSION

This paper gives an overview of the design of a shape-adaptive slat for scaled wind tunnel investigations at a wind energy profile. Based on the given geometry and requirements the structural concept of the slat is developed and described. In order to improve the fatigue behaviour of the slat's wind tunnel model the suction side's skin of the slat is designed in a parameter study with the objective to reduce the resultant strains in case of a deformed slat. In the case of a completely closed gap a maximum strain $\varepsilon_{close}$ of 0.34 % results. The fatigue strength of the wind tunnel model is proven with experimental fatigue investigations with up to $1 \cdot 10^6$ cycles. Finally the wind tunnel model with the shape-adaptive slat and the corresponding kinematics is manufactured and presented.

As a next step the hardware to drive the stepping motors will be modified for controlled shape actuations. After that a wind tunnel campaign with controlled shape actuations as reaction of turbulent inflow conditions which are generated by an active grid will be done.

Furthermore, investigations to transfer the developed concept of the scaled slat to a full-scale slat are planned. Based on the changed dimension the main objective is to check the full-scale suitability of the selected concept and actuators. Another objective of interest is to use GFRP instead of metal as the slat's material.

## ACKNOWLEDGEMENTS

This work was funded by the German Ministry of Economic Affairs and Energy (BMWi) on decision of the German Bundestag in the frame of the SmartBlades project (funding reference no. 0325601A/B/C/D).

## REFERENCES

[1] Berry, D., *Design of 9-Meter Carbon-Fiberglass Prototype Blades: CX-100 and TX-100*, Sandia Report SAND2007-0201, USA, 2007.

[2] Ashwill, T., *Passive Load Control for Large Wind Turbines*, Sandia Report SAND2010-3276C, USA, 2010.

[3] Barlas, T.K. and van Kuik, G.A.M., *Review of state of the art in smart rotor control research for wind turbines*, Progress in Aerospace Science (2009), doi:10.1016/j.paerosci.2009.08.002, 2009.

[4] Barlas, A., Aagaard Madsen, H., Løgstrup Andersen, T., *Design and simulation of the rotating test rig in the INDUFLAP project*, DTU Wind Energy. (DTU Wind Energy E; No. 0063(EN)), 2014.

[5] Barlas, A., Bergami, L., Hansen, M.H., Pedersen, M.M., Verelst, D.R., Thomsen, K. Aagaard Madsen, H. *Load alleviation potential of active flaps and individual pitch control in a full design load basis*, In Proceedings of the EWEA Annual Event and Exhibition 2015, European Wind Energy Association (EWEA), 2015.

[6] Aagaard Madsen, H., Barlas, A., Løgstrup Andersen, T. *Testing of a new morphing trailing edge flap system on a novel outdoor rotating test rig*, In Scientific Proceedings, EWEA Annual Conference and Exhibition 2015. (pp. 26-30). European Wind Energy Association (EWEA), 2015.

[7] Berg, J. and Barone, M. and Resor, B. *Field Test Results from the Sandia SMART Rotor*, 51st AIAA Meet, AIAA 2013-1060, Texas, 2013.

[8] Pechlivanoglou, G. and Wagner, J. and Nayeri, C. and Paschereit, C., *Active aerodynamic control of wind turbine blades with high deflection flexible flaps*, in AIAA 2010-644, 48th AIAA Aerospace Sciences Meeting Including the New Horizons Forum and Aerospace Exposition, Orlando, Florida, USA 2010.

[9] Berg, D.E., Wilson, D.G., Resor, B.R., Barone, M.F., Berg J.C., Kota, S. and Ervin, G.*Active Aerodynamic Blade Load Control Impacts on Utility-Scale Wind Turbines*, Sandia National Laboratories, FlexSys Inc., 2009.

[10] Subramanian, B. and Kirtley, K. R. and Standish, K. J., *Method and apparatus for increasing lift on wind turbine blade*, Patent Application, No. US2010/0143152 A1.

[11] Larsen H., Mueller J.A., Larsen, L., *Blade for a rotor of a wind or water turbine*, Patent Application, No. WO2009/143846 A1.

[12] Mickeler, S., *Rotor blade for a wind power plant and wind power plant*, Patent application, No. WO 2009/146810 A2.

[13] Timmer, W.A. and van Rooij R.P.J.O.M., *Summary of the Delft University Wind Turbine Dedicated Airfoil*, Journal of Solar Energy Engineering, Vol. 125, Issue 4, Pages 488-496, Nov. 26 2003.

[14] Pechlivanoglou, G., Nayeri, C. N. and Paschereit, C. O., *Fixed leading edge auxiliary wing as a performance increasing device for hawt blades* DEWEK, Bremen, Germany, 2010.

[15] Gaunaa, M. and Zahle, F. and Sørensen, N. and Bal, C., *Quantification of the Effects of Using Slats on the inner Part of a 10MW Rotor*, EWEA 2012-European Wind Energy Conference & Exhibition, 2012.

[16] Monner, H.P., Huxdorf, O., Pohl, M., Riemenschneider, J., Homeyer, T. and Hölling, M. *Smart structures for wind energy turbines*, 25th AIAA/AHS Adaptive Structures Conference, AIAA SciTech Forum, AIAA 2017-0295, Grapevine, Texas, USA, 2017.

[17] Manso Jaume, A. and Wild, J., *Aerodynamic Design and Optimization of a High-Lift Device for a Wind Turbine Airfoil*, Springer Verlag. Pages 859-869, ISBN 978-3-319-27278-8.

[18] Gramüller, B., *Pressure-actuated Cellular Structures*, Dissertation, German Aerospace Center, Institute of Composite Structures and Adaptive Systems, Braunschweig, 2016.

[19] Vasista, S. and Tong, L., *Topology-Optimized Design and Testing of a Pressure-Driven Morphing-Aerofoil Trailing Edge Structure*, AIAA Journal, Vol. 51, No. 8 (2013), Pages 1898-1907.

[20] Krone, J.H., Huxdorf, O., Riemenschneider, J., Monner, H.P., Schur, F., Friedrichs, J. and Wiedemann, M., *Experimental investigation and design of a shape-variable compressor cascade*, CEAS Aeronautical Journal, doi:10.1007/s13272-016-0224-1, 2016.

[21] Monner, H. P., *Realization of an optimized wing camber by using formvariable flap structures*, Aerospace Science and Technology, Volume 5, Issue 7, Pages 445-455, 2001.

[22] GOM GmbH *ARAMIS - 3D Motion and Deformation Sensor*, `http://www.gom.com/metrology-systems/aramis.html`.

[23] Wittel, H. and Muhs, D. and Jannasch, D. and Voßiek, J., *Roloff/Matek Maschinenelemente*, 19th. edition, Vieweg + Teubner, Wiesbaden, 2009.